



What is the limit of climate engineering by stratospheric injection of SO₂?

U. Niemeier and C. Timmreck

Max Planck Institute for Meteorology, Bundesstr. 53, 20146 Hamburg, Germany

Correspondence to: U. Niemeier (ulrike.niemeier@mpimet.mpg.de)

Received: 1 April 2015 – Published in Atmos. Chem. Phys. Discuss.: 15 April 2015

Revised: 31 July 2015 – Accepted: 3 August 2015 – Published: 18 August 2015

Abstract. The injection of sulfur dioxide (SO₂) into the stratosphere to form an artificial stratospheric aerosol layer is discussed as an option for solar radiation management. The related reduction of radiative forcing depends upon the injected amount of sulfur dioxide, but aerosol model studies indicate a decrease in forcing efficiency with increasing injection rate. None of these studies, however, consider injection rates greater than 20 Tg(S) yr⁻¹. But this would be necessary to counteract the strong anthropogenic forcing expected if “business as usual” emission conditions continue throughout this century. To understand the effects of the injection of larger amounts of SO₂, we have calculated the effects of SO₂ injections up to 100 Tg(S) yr⁻¹. We estimate the reliability of our results through consideration of various injection strategies and from comparison with results obtained from other models. Our calculations show that the efficiency of such a geoengineering method, expressed as the ratio between sulfate aerosol forcing and injection rate, decays exponentially. This result implies that the sulfate solar radiation management strategy required to keep temperatures constant at that anticipated for 2020, while maintaining business as usual conditions, would require atmospheric injections of approximately 45 Tg(S) yr⁻¹ (±15% or 7 Tg(S) yr⁻¹) at a height corresponding to 60 hPa. This emission is equivalent to 5 to 7 times the Mt. Pinatubo eruption each year.

pact of SRM, model comparison studies have been performed (Kravitz et al., 2011) to simulate mirrors in space (e.g., Schmidt et al., 2012) or stratospheric injection of sulfur dioxide (e.g., Pitari et al., 2013). Such injections, first suggested by Budyko (1977) and later by Crutzen (2006), follow the example of volcanic eruptions that naturally emit large amounts of SO₂ above the tropopause. Chemical and microphysical reactions in this region result in the formation of sulfate aerosols that reduce through solar reflection the available solar radiation at the earth’s surface, and absorb outgoing longwave radiation in the stratosphere.

Initial studies of artificial sulfate aerosols estimated their effect on climate by performing climate model simulations with prescribed particle size and relatively vague assumptions for aerosol particle evolution (Rasch et al., 2008; Robock et al., 2008; Tilmes et al., 2009). A more comprehensive study, albeit two-dimensional, using a sectional aerosol microphysical model showed that the particle size distribution of the sulfate aerosol cloud depended strongly on the magnitude of the injections (Heckendorn et al., 2009) which has been confirmed by later studies (Pierce et al., 2010; Niemeier et al., 2011; Hommel and Graf, 2011; English et al., 2012). However, the results differ in detail, in the simulated particle size distribution and in the poleward transport of stratospheric aerosol particles. These differences have implications for the estimated radiative forcing and hence the impact of the stratospheric aerosols on the climate and ozone concentration.

These previous studies were performed with SO₂ injections in the range of 1 to 20 Tg(S) yr⁻¹. Earth system model studies, which try to counteract anthropogenic GHG forcing to maintain 2020 forcing conditions within the Geoengineering Model Intercomparison Project (GeoMIP, Kravitz et al.,

1 Introduction

Climate engineering (CE) aims to counteract anthropogenic forcing due to greenhouse gas (GHG) emissions by reducing the amount of incoming solar radiation through solar radiation management (SRM). To estimate the climate im-

2011), estimated sulfur injection rates within this range. For example Niemeier et al. (2013) previously used up to 6 Tg(S) yr^{-1} to counteract 1.5 W m^{-2} forcing of GHG as prescribed in the RCP4.5 scenario, defined in the fifth phase of the Climate Model Intercomparison Protocol (CMIP5, Taylor et al., 2012), for the second half of this century. Counteracting the forcing of the stronger GHG scenario RCP8.5 will require higher SO_2 injection rates.

With increasing injection rate the forcing efficiency, the ratio of sulfate aerosol forcing to injection rate, decreases (Heckendorn et al., 2009). This decrease in forcing efficiency is non-linear and the injected SO_2 amount needed to reduce strong GHG forcings will be high. This raises the question of whether or not it will be possible to counteract strong GHG forcing, like the RCP8.5 scenario, for example, down to a level anticipated for 2020. This would require a reduction of -5.5 W m^{-2} in 2100. Therefore, we try to estimate a theoretical upper limit for possible SO_2 injections after which a further increase in injection rate causes only a negligible decrease in radiative forcing.

We have performed simulations with the middle atmosphere version of the general circulation model (GCM) ECHAM5 (Roeckner et al., 2006; Giorgetta et al., 2006) interactively coupled to a modified version of the aerosol microphysical model HAM (Stier et al., 2005). This three-dimensional modal aerosol model allows for dynamical feedback on particle distribution. Particle size is a crucial parameter for the effectiveness of stratospheric aerosols as it influences absorption and scattering properties as well as the sedimentation velocity. The model is not coupled to an ocean model, nor to a full atmospheric chemistry module. Thus, impacts on climate or ozone concentrations were not simulated.

ECHAM5-HAM simulations of injection rates up to $100 \text{ Tg(S) yr}^{-1}$ will be analyzed with respect to the efficiency of the injections (Sect. 3.1) followed by a discussion about injection strategies such as modification of the injection area size and different model configurations (Sect. 3.2). We compare our results in Sect. 3.3 to those obtained from other models (Heckendorn et al., 2009; Pierce et al., 2010; English et al., 2012) to provide a broader perspective. In Sect. 4 we consider the limitations of SO_2 injection and give rough estimates of possible impacts of such a strong SO_2 injection required to counteract a GHG forcing of 5.5 W m^{-2} , which would be necessary to reduce RCP8.5 anthropogenic forcing to a level anticipated for the year 2020 in years 2100 and later.

2 Description of the model and the performed simulations

2.1 Model setup

The simulations for this study were performed with the middle atmosphere version of the GCM ECHAM5 (Giorgetta

et al., 2006) with a spectral truncation at wave-number 42 (T42) and 39 vertical layers up to 0.01 hPa. The GCM solves prognostic equations for vorticity, divergence, surface pressure, water species, and temperature. In the model version used the quasi-biennial oscillation (QBO) in the tropical stratosphere is not resolved and the model remains in a permanent east phase. The model runs in climate mode with fixed sea surface temperature.

The aerosol microphysical model HAM (Stier et al., 2005) is interactively coupled to the GCM, as well as to the radiation scheme of ECHAM5. The sulfate aerosol influences dynamical processes via temperature changes caused by scattering of shortwave radiation and absorption of near-infrared and longwave radiation. HAM calculates the sulfate aerosol formation including nucleation, accumulation, condensation and coagulation, as well as its removal processes via sedimentation and deposition. A simple stratospheric sulfur scheme is applied at the tropopause and above (Timmreck, 2001; Hommel et al., 2011). This scheme uses prescribed oxidant fields of OH, NO_2 , and O_3 on a monthly basis, as well as photolysis rates of OCS, H_2SO_4 , SO_2 , SO_3 , and O_3 . OCS concentrations are prescribed at the surface and transported within the model.

The microphysical core of HAM, M7 (Vignati et al., 2004), was modified to allow better representation of the stratospheric sulfate aerosol. Nucleation was adapted to high H_2SO_4 concentrations, so when the number of molecules in the critical cluster is small (< 4) the collision rate of two molecules is calculated and used instead of the nucleation rate (Vehkamäki et al., 2002). The time stepping scheme for the H_2SO_4 gas equation is solved as described in Kokkola et al. (2009), which increased the accuracy of the model compared to previous versions (Wan et al., 2013). Within this stratospheric HAM version we treat only the sulfate aerosol and, apart from the injected SO_2 , only natural sulfur emissions are taken into account in the simulations. Further details are described by Niemeier et al. (2009).

The original modal setup of M7, i.e., with seven modes, represents tropospheric conditions and is not representative of the stratospheric sulfate aerosol. In accordance with box-model studies (Kokkola et al., 2009) we applied a special setup of the modes to describe stratospheric sulfate aerosols: one for simulations of volcanic eruptions (Volc) and one for SRM (Geo). Both are used in this study. The volcanic setup (Volc) contains no coarse mode and a narrower accumulation mode (standard deviation $\sigma_{\text{AS}} = 1.2$). Model results using this setup show overall good agreement for particle size and radiation at the top of the atmosphere (TOA) with measured data taken after the Mt. Pinatubo eruption (Niemeier et al., 2009; Toohey et al., 2011). We see a slight overestimation of the poleward transport in the aerosol optical depth (AOD) compared to satellite measurements (Thomason et al., 1997), and, consequently, calculated aerosol concentrations in the tropics were lower than observed 6 months after the eruption. The simulated tracer transport into the Southern Hemisphere

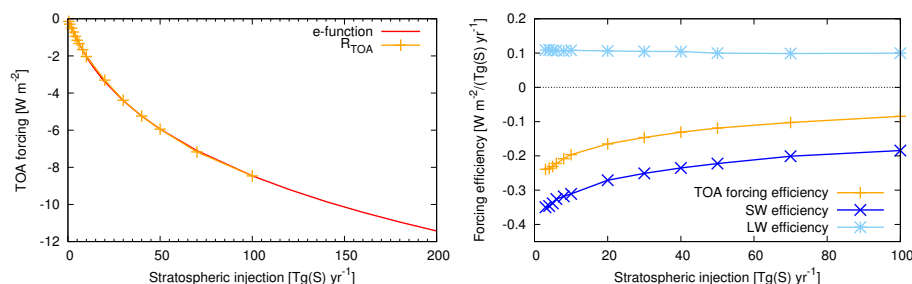


Figure 1. (Left) Top of the atmosphere (TOA) radiative fluxes (net shortwave plus net longwave, orange) for different injection rates (GeoX, Table 1) and exponential fit of TOA forcing (red) (Eq. 1). (Right) Forcing efficiency of TOA radiative forcing, forcing per injection [$\text{W m}^{-2} (\text{Tg(S) yr}^{-1})^{-1}$], for ΔR_{TOA} (orange), SW and LW radiation (blue).

after the Mt. Pinatubo eruption in June 1991 and the related AOD compare well with satellite measurements (Thomason et al., 1997).

For simulations of SRM with sulfate aerosols the modal setup of M7 was further optimized. The sectional aerosol model simulations (Heckendorn et al., 2009) show a wider size distribution for SRM than observed after a volcanic eruption, as the simulations of Kokkola et al. (2009) did for lower SO_2 concentrations. This reflects the smaller sulfur flux (continuous emission) compared to those required for volcanic eruptions. Based on these studies of the SRM distribution, the original ECHAM5-HAM distribution was changed to a smaller standard deviation of the coarse mode ($\sigma = 1.2$ instead of 2), while we kept the normal standard deviation of $\sigma = 1.59$ in the model code for the accumulation mode. As a result, the simulated particle number distributions compare better to those calculated by the sectional aerosol model of Heckendorn et al. (2009). This SRM setup was used to calculate the amount of SO_2 injections necessary to counterbalance anthropogenic forcing in the GeoMIP G3 experiment (Niemeier et al., 2013). The data from this model are used as input data for a GeoMIP intercomparison study (Tilmes et al., 2015).

2.2 Setup of simulations

To study the dependence of the particle size distribution on the amount of injected SO_2 , a series of numerical experiments were performed with injections between 1 and $100 \text{ Tg(S) yr}^{-1}$. SO_2 was injected continuously at a height of 60 hPa (about 19 km) into one grid box ($2.8^\circ \times 2.8^\circ$) centered at the Equator at 121° E . In addition to the geoengineering setup, we used the volcanic setup for $100 \text{ Tg(S) yr}^{-1}$ injection rate. All of the results presented here are averaged over at least 3 years of a steady global sulfur burden.

To estimate the uncertainty of the simulations, we varied the size of the injection area. For an injection rate of 10 Tg(S) yr^{-1} we increased the area of injections meridionally to 5° N and 5° S , and to 30° N and 30° S , as well as zonally to a one grid box wide circle along the Equator (Table 1). We also varied the injection height and performed

simulations with a second injection height of 30 hPa (about 24 km) for two different meridional extensions: the grid box and 30° N to 30° S . We did not alter the zonal position of the injection box because a case study by Toohey et al. (2011) revealed on average no significant longitudinal impact on tracer transport for a large tropical volcanic eruption.

3 Results

In this study we aim to determine the efficiency of stratospheric SO_2 injections and their dependency on the injection rate. The results are subject to several uncertainties, like the modal setup and influence of injection area. We estimate their importance and impact on the presented results within this section. The efficiency of SO_2 injections is the ratio of top of the atmosphere (TOA) forcing to injection rate.

3.1 Impact of increasing injection rate

Figure 1 (left) shows the simulated change in global radiative fluxes at the top of the atmosphere (TOA) for different SO_2 injection rates. These data are derived from running the radiation calculation in the model twice, once without and once with aerosols, whereby only the latter is used for the model integration. With this method we calculate the instantaneous aerosol forcing only. The orange curve shows the data for the TOA forcing (ΔR_{TOA}), net shortwave (SW) plus net longwave (LW) radiation, for the different injection rates. The simulations show a reduction of TOA forcing by -0.5 , -2 , -6 , -8.5 W m^{-2} for injection rates of 2, 10, 50, $100 \text{ Tg(S) yr}^{-1}$, respectively. The red curve in Fig. 1 (left) is a fit of the ΔR_{TOA} as function of injection rate x (in Tg(S) yr^{-1}):

$$\Delta R_{\text{TOA}} = -65 \text{ W m}^{-2} \cdot e^{-\left(\frac{2246 \text{ Tg(S) yr}^{-1}}{x}\right)^{0.23}}. \quad (1)$$

This fit to the simulated TOA imbalance extrapolates the simulated ΔR_{TOA} for even higher injection rates. Upon doubling the injection rate from 100 to $200 \text{ Tg(S) yr}^{-1}$ the fitted exponential function yields an increase in the negative forcing

Table 1. Overview of the input parameters for the simulations performed with ECHAM5-HAM. The injection rate differs between the simulations, as well as the injection area and injection height and the mode configuration of the aerosol microphysics. Lonbox is one grid box at the Equator at 120.9 to 123.75° E. GeoX is a synonym for the injection rates of 1 to 100 Tg(S) yr⁻¹.

Simulation	Rate Tg(S) yr ⁻¹	Area	Height	Mode setup
GeoX	1, 2, 3, 4, 5, 6, 8, 10, 20, 30, 40, 50, 70, 100	2.8° N to Eq. lonbox	60 hPa	geoeng. $\sigma_{AS} = 1.59, \sigma_{CS} = 1.2$
Geo10-5	10	5° N to 5° S lonbox	60 hPa	geoeng. $\sigma_{AS} = 1.59, \sigma_{CS} = 1.2$
Geo10-30	10	30° N to 30° S lonbox	60 hPa	geoeng. $\sigma_{AS} = 1.59, \sigma_{CS} = 1.2$
Geo10-lon	10	2.8° N to Eq. all longitudes	60 hPa	geoeng. $\sigma_{AS} = 1.59, \sigma_{CS} = 1.2$
Geo10-high	10	2.8° N to Eq. lonbox	30 hPa	geoeng. $\sigma_{AS} = 1.59, \sigma_{CS} = 1.2$
Geo10-30-high	10	30° N to 30° S lonbox	30 hPa	geoeng. $\sigma_{AS} = 1.59, \sigma_{CS} = 1.2$
Volc100	100	2.8° N to Eq. lonbox	60 hPa	volc. $\sigma_{AS} = 1.2$

from -8.5 to roughly -12 W m^{-2} . Doubling of the injection rate, therefore, results in an increase of only 40 % in the forcing.

A more detailed illustration of the radiative forcing efficiency at TOA is given in Fig. 1 (right), where the ΔR_{TOA} is split in a SW and LW part. This figure clearly depicts that the decreasing radiative forcing efficiency results from the SW part. An injection of 5 Tg(S) yr^{-1} yields an efficiency of $-0.23 \text{ W m}^{-2} (\text{Tg(S) yr}^{-1})^{-1}$, while an injection of 50 Tg(S) yr^{-1} yields an efficiency of $-0.12 \text{ W m}^{-2} (\text{Tg(S) yr}^{-1})^{-1}$: a 10-fold increase in injection rate results in a 50 % reduction in the efficiency. This result can be explained by Fig. 2. For small injection rates ($\leq 10 \text{ Tg(S) yr}^{-1}$) Fig. 2 shows that the number distribution is greater in accumulation mode than in coarse mode. As injection rates increase, particle number and radii increase stronger in coarse mode than in accumulation mode. With increasing particle size scattering becomes less effective. The parallel curves of SW and ΔR_{TOA} efficiency in Fig. 1 (right) indicate that the changes in scattering are mostly responsible for the decrease of ΔR_{TOA} efficiency. In contrast, efficiency of LW radiation at TOA is almost constant and positive at $0.1 \text{ W m}^{-2} (\text{Tg(S) yr}^{-1})^{-1}$. So the TOA LW flux anomalies are linearly dependent on the injection rate and contribute to the GHG effect instead of counteracting it.

Summarizing, the decrease in efficiency with increased injection rate follows exponential decay and is the consequence of the increased particle size that occurs with increased injection rate. Larger particle radii result in decreased scattering of SW radiation and a shorter lifetime of the sulfate aerosol

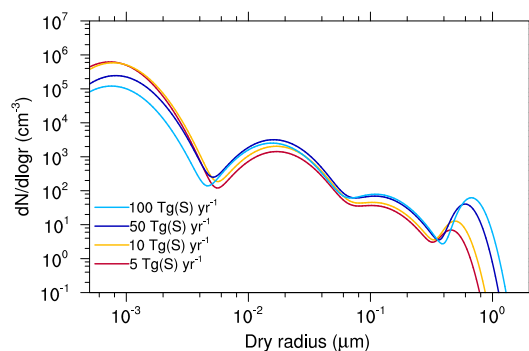


Figure 2. Zonally averaged aerosol number size distribution at 54 hPa height at the Equator for different injection rates. Given are values for nucleation mode (radius (r) ≤ 5 nm), Aitken mode ($5 \text{ nm} \leq r \leq 50 \text{ nm}$), accumulation mode ($0.05 \mu\text{m} \leq r \leq 0.2 \mu\text{m}$) and coarse mode ($r \geq 0.2 \mu\text{m}$). Only particles in accumulation and coarse modes are radiatively active. Scattering of SW radiation is strongest in accumulation mode and gets less effective with increasing particle size (Pierce et al., 2010).

(Niemeier et al., 2011). LW absorption by the sulfate aerosol scales linearly per injected mass.

3.2 Range of results within one model

In this section we investigate the robustness of the values given in Fig. 1. The general performance of the global aerosol model has already been discussed in Sect. 2. Here, we test the robustness of our results by varying the injection area and by changing the internal M7 mode setup.

Table 2. Burden, AOD, ΔR_{TOA} (net SW + LW), and net surface SW radiation for the different simulations. ΔR_{diff} is the relative difference of ΔR_{TOA} to Geo10 and Geo100. Geo10 and Geo100 follow the design of GeoX (Table 1) with injection rates of 10 and 100 Tg(S) yr⁻¹.

Simulation unit	Burden Tg(S)	AOD	ΔR_{TOA} W m ⁻²	ΔR_{diff} %	SW_{srf} W m ⁻²
Geo10	6.44	0.18	-2.03	-	-2.55
Geo10-5	6.36	0.17	-2.06	-1.5	-2.52
Geo10-30	6.16	0.15	-1.81	-11	-2.3
Geo10-lon	5.98	0.14	-1.79	-12	-2.3
Geo10-high	10.01	0.24	-3.02	+50	-3.8
Geo10-30-high	9.56	0.22	-2.76	+36	-3.5
Geo100	62.3	0.79	-8.46	-	-14.9
Volc100	61.8	0.89	-9.01	6	-15.43

3.2.1 Impact of the size of the injection area – zonal extension

To further investigate the impact of the SO₂ injection flux per area the emission area was increased in longitudinal direction for an injection rate of 10 Tg(S) yr⁻¹. Table 2 gives the resulting global values of sulfur burden, AOD, top of the atmosphere forcing ΔR_{TOA} , and net SW radiation at TOA. The burden decreases with increasing emission area, as does AOD and ΔR_{TOA} . ΔR_{TOA} decreases by 12 % when SO₂ is injected zonally along the Equator (Geo10-lon) instead of into a single grid box. The reason can be found in aerosol microphysical as well as in dynamical differences (see below).

The temporal microphysical evolution of the stratospheric sulfate aerosol is a competing process between nucleation, coagulation and condensation. The amount of nucleation or coagulation depends on the SO₂ flux into the stratosphere, as well as on the amount of existing particle (Heckendorn et al., 2009). An important difference between a case study of an explosive volcanic eruption and of a sulfur SRM application, as considered here, is the continuous sulfur emission flux. In the latter freshly injected SO₂ is always available, which has the following consequences for the microphysical processes of aerosol development:

1. Nucleation continuously forms small particles within the injection area.
2. H₂SO₄ is always available within the injection area to condense on these particles, the first growth step within the nucleation and Aitken modes.
3. Due to advection, larger particles in accumulation and coarse mode are globally dispersed.
4. The coagulation coefficient depends on the ratio of radii between fine and coarse particles (Seinfeld and Pandis,

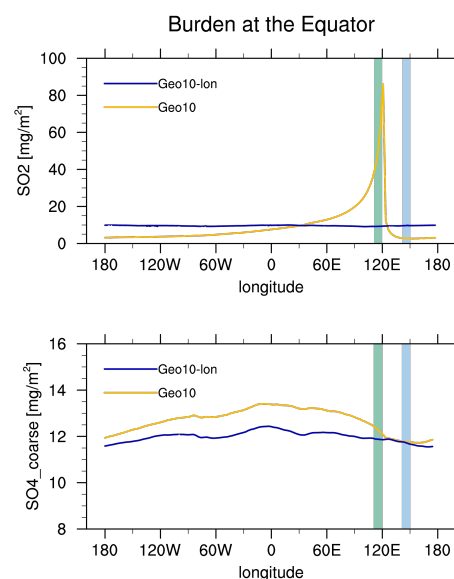


Figure 3. Burden of (top) SO₂ and (bottom) sulfate coarse-mode particles as calculated in the grid box along the Equator for two different simulations. Within the two marked areas concentrations are averaged for Fig. 4: downwind of the injection area at 110 to 120° E (green area, named AREA-115 later) and upwind to the injection area at 140 to 150° E (blue area, AREA-145). Meridionally both areas are one model grid box wide, from the Equator to 2.8° N.

1998). The larger the ratio, the larger is the coagulation coefficient. This is most effective between fine ($r < 0.01 \mu\text{m}$) and coarse particles ($r > 1 \mu\text{m}$). As a consequence of the continuous emission flux under sulfur SRM, large and fine particle sizes are always available. Hence coagulation has a stronger impact on particle size than condensation (Heckendorn et al., 2009) and is mostly responsible for the growth of coarse sized particles.

Figure 3 shows the distribution of SO₂ burden (top) and coarse-mode sulfate particle burden (bottom) along the Equator for simulations Geo10 and Geo10-lon. For Geo10 the SO₂ burden is high within the injection area and SO₂ is advected to the west with burden values declining steeply. In Geo10-lon the constant emissions along the Equator result in an equal burden of about 10 mg m⁻³ of SO₂. This is almost one order of magnitude smaller than the maximum in Geo10 and an order of magnitude larger than the minimum in Geo10 upwind of the injection area around AREA-145. H₂SO₄ and nucleation mode particles behave similarly to SO₂ and occur mostly in the injection area as conversion processes occur quickly. In contrast to the distribution of precursor gases and the particles in the nucleation mode, the distribution of the coarse-mode particles along the Equator in both simulations is almost equal (Fig. 3, bottom). This indicates that the lifetime of the coarse particles is longer than the zonal mixing time due to advection and diffusion and that transport plays

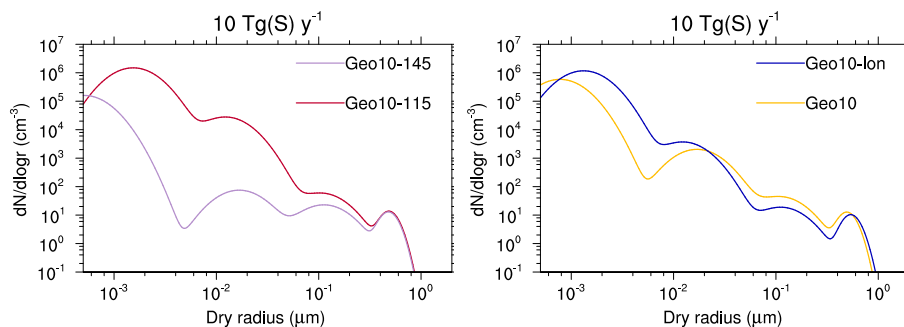


Figure 4. Aerosol number size distribution of particles in a height of 54 hPa at the Equator for injection rates of 10 Tg(S) yr^{-1} . (Left) Geo10 averaged over a 10° wide area upwind (Geo10-145) and downwind (Geo10-115) of the injection area (see also Fig. 3). (Right) Zonal average of Geo10 and Geo10-lon.

an important role for the larger particles. The distribution in the stratosphere of nucleation and Aitken mode particles is mainly determined by microphysical processes, while accumulation and coarse-mode particle distributions depend on both microphysical processes and on transport.

Figure 4 shows on the left the aerosol number size distribution of Geo10 as an average over the downwind grid box AREA-115 (see Fig. 3) and the upwind grid box AREA-145, and on the right the zonal average of Geo10 and Geo10-lon at the Equator. Compared to AREA-145 the number size distribution of AREA-115 shows high particle numbers in all modes, indicating that the processes of nucleation, condensation and coagulation are all in operation, especially new particle formation. In AREA-145 SO_2 concentration is low; consequently, the nucleation particle number and radius are both small. Additionally, low Aitken and accumulation mode numbers indicate small amounts of nucleation and condensation. This shows that the process of particle growth occurs mostly in, and downwind of, the injection area. In Geo10-lon injections occur along the Equator. The size number distribution of the zonal average, here representative of the injection area, is very similar to the one of AREA-115. For Geo10-lon both fine and large particles are available at all longitudes (Fig. 3) and the ratio of fine to large radii is large everywhere. Coagulation is, therefore, the dominant process everywhere and particles are able to grow in size. This decreases SW scattering and hence the forcing efficiency, by -12% in ΔR_{TOA} (Sect. 3.1).

Earlier studies (Heckendorn et al., 2009; Niemeier et al., 2011) suggest a similar effect when prolonging the time period of stratospheric injections. Changing the injection period from pulse to continuous decreases the injection flux but results over time in a more even distribution of particles and an overall quite regular availability of small particles. This results in a change in efficiency of -3% (Niemeier et al., 2011).

3.2.2 Impact of the size of the injection area – vertical shift

To investigate the impact of the injection height, we shifted the area from a height corresponding to 60 hPa to 30 hPa (about 24 km) and performed two simulations: Geo10-high, the same design as Geo10 with different injection height only, and Geo10-30-high using the design of Geo10-30 with an injection area between 30° N and 30° S .

Geo10-high shows an increase in efficiency by 50%. The main reason for this increase is the longer sedimentation path through the stratosphere and the resulting larger AOD in the stratosphere. It simply takes longer, until the sulfate reaches the troposphere, where wet deposition is strong and sulfate removed quickly. A second reason is a slight difference in transport due to differences in meridional transport at different heights. Meridional transport out of the tropics is stronger in the lower stratosphere, while vertical transport gets stronger in the middle stratosphere. This causes an additional vertical extension of the sulfate layer in Geo10-high and increases the AOD further (Fig. 5, right).

3.2.3 Impact of the size of the injection area – meridional extension

The effect of increasing the size of the injection area meridionally was considered in simulations Geo10-5, Geo10-30 and Geo10-30-high (Table 1). For Geo10-5 the injection area is 4 times larger than for Geo10, for Geo10-30 20 times larger. The number size distribution in Fig. 5 (left) shows smaller values for the Aitken and accumulation modes for Geo10-30. This indicates a slight increase of coagulation in Geo10-30, resulting in a slight increase of the final particle size of the coarse mode.

The zonally averaged AOD (Fig. 5, right) reveals clear differences in the meridional distribution of sulfate in Geo10-30 compared to Geo10 and Geo10-5. The equal distribution of the injection over more latitudes reduces tropical AOD. The meridional cross sections of the zonal and annual mean of the SO_2 and sulfate concentrations (Fig. 6)

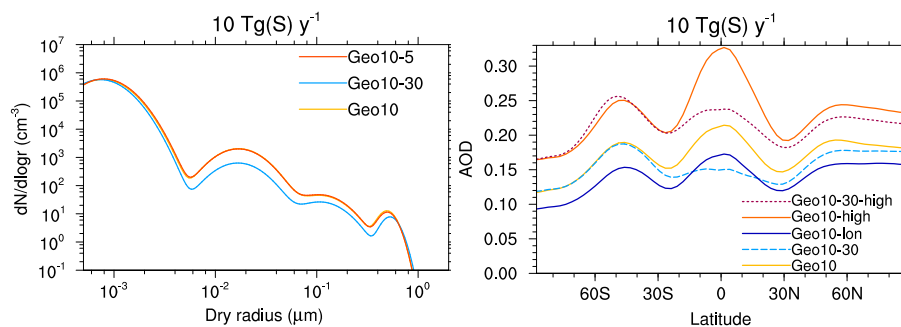


Figure 5. (Left) Aerosol number size distribution as in Fig. 4, but for the meridionally extended regions (Geo10-5, Geo10-30) and (right) zonally averaged data of AOD for experiments with injection rates of 10 Tg(S) yr^{-1} and varying extent of the injection area in zonal (Geo10-lon) and meridional (Geo10-5, Geo10-30) directions, and increasing injection level (Geo10-high, Geo10-30-high).

show clear differences in the vertical distribution of SO_2 between Geo10 and Geo10-30. The temperature within the sulfate cloud is higher and the vertical velocity is about 10% larger in Geo10 than in Geo10-30. The consequence is an increased vertical transport of the aerosols in the tropical stratosphere. The difference in the SO_2 and aerosol distribution is further related to stratospheric dynamics. At the boundary of the tropical region a subtropical transport barrier hinders meridional mixing (Brasseur and Solomon, 2005). Previous ECHAM5 results indicate that this transport barrier in a simulation without quasi-biennial oscillation is strongest around the latitude of 10° in the summer hemisphere (Punge et al., 2009). In Geo10-30 parts of the SO_2 emissions are outside of this barrier; thus, meridional transport of SO_2 is greater (Fig. 6). Comparing the two cases with higher level injections (Geo10-high and Geo10-30-high) this behavior is even more obvious. In the extra-tropical region of the Southern Hemisphere the AOD in Geo10-30-high is greater than the AOD of Geo10-high, indicating stronger transport. The smaller tropical AOD, however, causes a smaller global value than in Geo10-high.

In summary, decreased efficiency is observed when the injection area is increased zonally. This causes a more even spread of precursor gases and fine particle. Coagulation is increased and this results in the formation of larger particle radii and decreased SW scattering. The tropical transport barrier is an important factor when increasing the meridional injection area. Injecting outside of this barrier increases meridional transport and decreases the lifetime of the sulfate aerosol.

3.2.4 Impact of the modal setup of HAM and the applied model configuration

HAM is a modal aerosol model, in which the aerosol size is simplified by the use of four log-normal distributions. Therefore, we have considered the uncertainty range related to the modal setup of our model. Additional, we discuss the impact of the vertical model resolution on the results.

Weisenstein et al. (2007) compared a modal aerosol model with a fine bin model showing that with an optimized mode width, a modal model can reasonably describe the distribution of a bin model. English et al. (2013) highlighted the changing mode width over time after a volcanic eruption. This changing time factor is not important under SRM as the size distribution is in equilibrium. These results show, however, that different injection rates affect the mode distribution. Kokkola et al. (2009) compared in a box model study complex aerosol bin models with different modal setups of M7, the microphysical core of HAM. The results of the bin models showed that upon increasing the initial SO_2 concentration from 10^{-8} to $10^{-6} \text{ kg kg}^{-1}$ the number distribution for radii $r > 0.1 \mu\text{m}$ becomes mono-modal with a narrower mode width compared to standard M7. Consequently, the simulation of a volcanic eruption with very high initial SO_2 concentrations required the development of parameters particular for this situation (Sect. 2). In Geo100, with a continuous injection rate of $100 \text{ Tg(S) yr}^{-1}$, the mean SO_2 concentration in AREA-115 is $3.5 \times 10^{-6} \text{ kg kg}^{-1}$, which is within the range of large volcanic eruptions.

To estimate the resultant uncertainty, a simulation with the mono-modal volcanic setup for an injection rate of $100 \text{ Tg(S) yr}^{-1}$ (Volc100) was performed. Although the number size distribution between both modal setup differs, the difference in global AOD is only about 10% and even less for ΔR_{TOA} and the sulfur burden (Table 2). So although the efficiency of injections of approximately $100 \text{ Tg(S) yr}^{-1}$ may be slightly underestimated with the chosen setup, the TOA imbalance stays within the uncertainty range given for the different Geo10 experiments. We concluded that our chosen mode distribution is reasonably accurate for a sensitivity study of different injection rates.

This study was performed with a relative coarse vertical resolution of 39 levels up to 0.01 hPa with stratospheric layers of 1.4 to 1.9 km depth. Increasing the number of vertical levels and, consequently, reducing the vertical grid spacing would slightly increase efficiency due to less numerical dif-

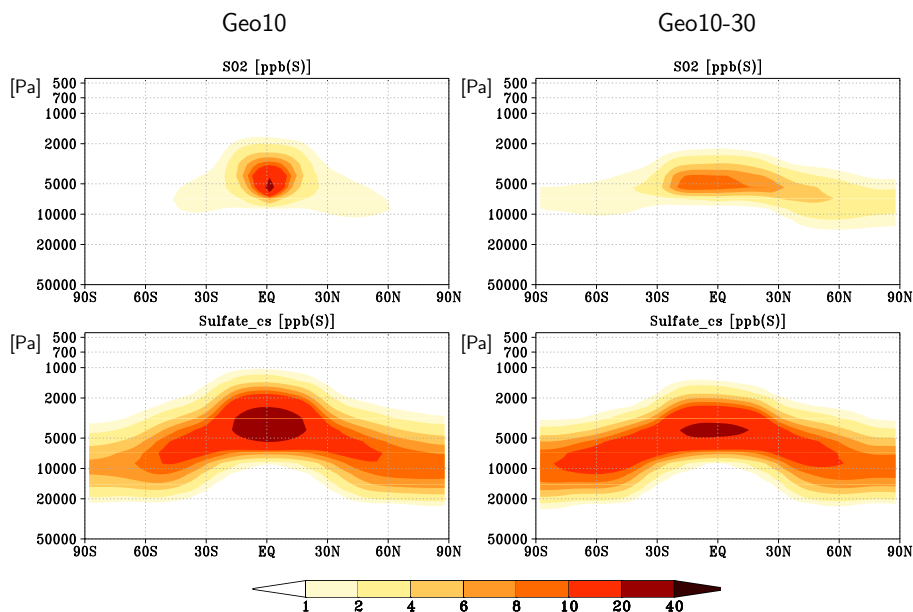


Figure 6. Zonally and annually averaged SO_2 (top) and sulfate coarse mode (bottom) concentration for Geo10 (left) and Geo10-30 (right) experiments with injection rates of 10 Tg(S) yr^{-1} .

fusion (3 % higher burden estimated from a volcanic eruption study).

Adding the QBO via nudging may also impact efficiency. Punge et al. (2009) show that methane concentrations in the tropics change by $\pm 10\%$ and by up to $\pm 15\%$ in extratropical regions depending on the QBO phase. These differences are caused by the different meridional transport resulting from the different stratospheric transport barrier strengths between the east and west phases of QBO (Plumb and Bell, 1982). A detailed analysis of the QBO impact on the tropical stratospheric aerosol layer was recently published by Hommel et al. (2015). Comparing simulations with and without QBO they found only moderate statistically significant QBO signatures ($< 10\%$) in the bulk of the stratospheric aerosol layer for most of the analyzed parameters (including the effective radius). Simulating an internally generated QBO-like oscillation by increasing the vertical resolution to 90 levels would cause a slowing of the QBO oscillation and for injection rates roughly about 8 Tg(S) yr^{-1} a constant QBO west phase in the lower stratosphere with overlaying easterlies (Aquila et al., 2014). Increasing injection rates strengthen the constant QBO west phase and decrease efficiency further by reducing the meridional transport.

3.3 Comparison to other studies

Comparison of the ECHAM5-HAM results to those from other models is limited by the fact that a range of slightly different SRM experiments has been performed. The experiments differ in size and height of injection area and the studies determine different parameters. Comparison is, there-

fore, difficult and we limit ourselves to sulfur burden and AOD. We have compared our 3-D interactive GEO1-10 simulations with the results of three other studies using two different aerosol models:

1. Pierce et al. (2010) (P10 thereafter) and Heckendorn et al. (2009) (denoted H09 hereafter) used AER-2D (Weissenstein et al., 2007), a 2-D sectional model. The aerosol is coupled to a radiation scheme in the climate model while aerosol microphysics were calculated in a 2-D model with fixed circulation without coupling to radiative effects.
2. English et al. (2012) (denoted E12 hereafter) used WACCM/CARMA which incorporates a 3-D sectional aerosol model without coupling to a radiation scheme.

The different treatments of the aerosol (2-D vs. 3-D, sectional vs. modal) impact tracer transport and particle size, while feedback from aerosol heating on tracer transport is only available from ECHAM5-HAM. These experiments encompass the range of the uncertainties in the modeling of the relationship between SO_2 injection and TOA forcing.

Figure 7 (left) shows the global sulfate aerosol burden for the ECHAM5-HAM simulation (Geo1 to Geo10), as well as results of SRM studies by P10 and E12. Both studies include data for two injection areas: between 5° N to 5° S (SO_2 -NARROW) and 30° N to 30° S (SO_2 -BROAD). In addition, the injection height was increased, from 20 km in SO_2 -NARROW to 20–25 km in the SO_2 -BROAD simulations. The global burden values of ECHAM5-HAM Geo1 to Geo10 are quite similar to SO_2 -NARROW results of P10

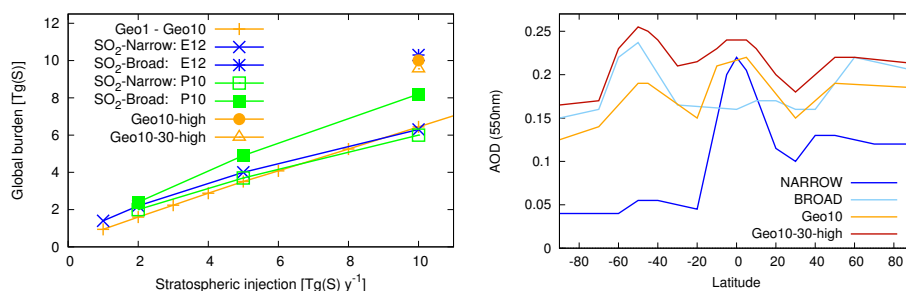


Figure 7. (Left) The global sulfate aerosol burden for ECHAM5-HAM simulations Geo1 to Geo10 compared with results from Pierce et al. (2010), P10, and English et al. (2012), E12, for two different emission areas: SO₂-NARROW, 5° N to 5° S, and SO₂-BROAD, 30° N to 30° S. In the SO₂-BROAD simulation the injection area is additionally increased vertically to 20–25 km. (Right) Plots comparing the zonal mean of the AOD for a narrow and a broad injection area. Plots were created using smoothed values of Geo10 and Geo10-30-high and estimated from “SO₂ NARROW” and “SO₂ BROAD” data after English et al. (2012).

and E12, with a slightly greater slope in ECHAM5-HAM. Increasing the injection height in ECHAM5-HAM shows a strong increase in the burden of 50 %, while an additionally meridionally increased injection area decreases this to 36 % over Geo10. Comparing to E12 and P10 we see a slightly stronger increase of the burden in E12 and a smaller increase in P12. The global burden of narrow simulations is rather similar in all three models and we assume that in P10 and E12 also the increase of the injection height causes the main increase in burden in the SO₂-BROAD simulations.

Global and meridional pattern of other variables, AOD and SW flux, are less similar between models, which we attribute to stratospheric transport. In Sect. 3.2.3 the importance of the tropical transport barrier on the tracer transport is discussed and from the results in H09, P10 and E12 we assume a stronger barrier is present in both models. To show the differences between the results obtained from a model incorporating a stronger transport barrier we show a schematic diagram of the zonally averaged AOD obtained for a narrow and a broad injection area (Fig. 7, right). Plots were created using values of Geo10 and Geo10-30-high and estimated from “SO₂ NARROW” and “SO₂ BROAD” data after Fig. 9 in E12 (here named NARROW and BROAD) – secondary minima and maxima were smoothed to provide a better overview. Both narrow cases (Geo10 and NARROW) show a distinct peak in the tropics suggesting a transport barrier in the tropical stratosphere stronger in NARROW than that found in Geo10. The broad cases show a greater distribution of sulfate aerosol over all latitudes and for BROAD higher AOD at mid latitudes and polar regions than for NARROW. This shift of high AOD values from the tropics to mid latitudes indicates increased meridional transport in BROAD compared to NARROW.

It is important, therefore, to consider whether or not SO₂ is injected inside or outside the tropical transport barrier and how the permeability and the width of the barrier influence the meridional transport in the model. Heating of the sulfate aerosol is not incorporated into E12 and it is difficult

to estimate its effect on results. Niemeier et al. (2011) show less vertical transport in the tropics when switching off the coupling of aerosols to radiative processes. Geo10-high and Geo10-30-high show that the main positive impact on efficiency is the increase in injection height. The increase of the area in meridional directions decreases the efficiency. We assume this is also a valid explanation for the difference between NARROW and BROAD simulations.

4 Limit, uncertainties, and consequences of strong sulfur injections

The performed simulations have not given a final answer on the limit of SO₂ injections. The fitted curve in Fig. 1 describes an exponential decay and converges to -65 W m^{-2} , which is a high and uncertain theoretical limit, only achievable with infinitely high injections being technically impossible. This limit is estimated for the chosen setup of injecting SO₂ into one grid box at the Equator at a height of 60 hPa and might not be valid anymore, if the injection strategy changes. Therefore, we tried to estimate different uncertainties by investigating different experiment designs. These simulations show that increasing the injection height has the strongest impact on our results. Increasing the injection height by 5 km would increase efficiency by 50 %. Increasing the area from one grid box in longitudinal direction reduces efficiency by up to -12% and by -11% when increasing the area meridionally (Table 2). We also examined the impact of the modal concept of aerosol microphysics and the number of vertical levels. None of these would impact the result by more than $\pm 15 \%$. Comparing to other studies showed similar sulfate burdens, but differences in the meridional distribution of the AOD mostly due to differences in the simulation of the stratospheric transport.

Reducing TOA forcing to counteract RCP8.5 anthropogenic forcing towards the end of the century to a level anticipated for 2020 would require a negative forcing of about 5.5 W m^{-2} or an injection of 45 Tg(S) yr^{-1} . This is about

85 % of the anthropogenic sulfur emissions in 2010 (Klimont et al., 2013). Compared to volcanic dimensions, this corresponds to approximately 6 to 7 Mt. Pinatubo eruptions per year – with 7 to 8 Tg(S) being the strongest eruption in the last century. Increasing the injection height from 19 to 24 km would increase efficiency by 50 % and reduce the required amount of SO₂ to 30 Tg(S) yr⁻¹, although this would be much more technically challenging. Following McClellan et al. (2012), existing planes would require technical changes to reach a height of 18 to 20 km, while higher injection levels might only be achieved by newly developed technology like hybrid air ships.

What would be the consequences of a 5.5 W m⁻² reduction of the forcing, when counteracting RCP8.5 in 2100 toward the forcing of 2020? Side effects may occur as a consequence of reduced amount of incoming SW radiation at the surface but also from changing indirect radiation, for example, on the growth rate of plants. Here we discuss some of these possible consequences, taken from previous studies and extrapolated for high injection rates.

Reducing the TOA forcing by 5.5 W m⁻² would result in a reduction of surface solar radiation by 7 to 8 W m⁻², an overall 4 % decline (Liepert, 2002) resulting in a reduction of evaporation and precipitation. The multi-model ensemble in Schmidt et al. (2012) allows an estimate of the precipitation change per reduced W m⁻² TOA forcing: about 0.035 mm day⁻¹ (W m⁻²)⁻¹, assuming a linear relation between precipitation change and TOA forcing. A -5.5 W m⁻² reduction in SRM forcing reduction would result in a decrease in the mean global precipitation by 0.19 mm day⁻¹, or -6.3 % of precipitation in RCP8.5 (2100) which is stronger than the increase in RCP8.5 since preindustrial conditions. This estimate does not include the even stronger reduction of precipitation under sulfate SRM (Niemeier et al., 2013). Additionally, much larger changes would be expected regionally.

Additional nuclei for cloud condensation may get into the upper troposphere via sedimentation of sulfate aerosols. The resulting brighter clouds might reflect more sunlight, a positive feedback that would provide some additional cooling. Cirisan et al. (2013) describe the mid-latitude averages in the range of ±0.04 W m⁻² for injection rates up to 5 Tg(S) yr⁻¹. Locally these values can be larger, but the overall global impact is small for larger injection rates as well. Furthermore, Kuebbeler et al. (2012) showed that a vertical shift of the tropopause height caused by the warmer lower stratosphere has implications on cirrus clouds and the cloud top height, with further impacts on the hydrological cycle.

Injecting SO₂ into the stratosphere also has consequences for the concentration of stratospheric ozone. Satellite observations after the Mt. Pinatubo eruption showed a decrease of 10 % in polar ozone concentration and ±2 % over the tropics (Randel et al., 1995), a value also simulated by different model studies. Previous geoengineering studies that included ozone chemistry estimated changes over the polar

region of -10 % for an injection of 2 Tg(S) yr⁻¹ (Tilmes et al., 2008) and around -5 % in a multi-model ensemble for 4 to 6 Tg(S) yr⁻¹ (Pitari et al., 2013). Both studies show a slight increase of ozone concentration over the tropics. For greater injection rates only studies on super volcano eruptions can be taken as references. Timmreck and Graf (2006) calculated height-dependent ozone changes within the stratosphere of +100 % (lower stratosphere) and -25 % in the tropics for a Yellowstone eruption of 850 Tg(S). Bekki et al. (1996) calculated for a simulation of the Toba eruption (about 3000 Tg(S)) a decrease of 40 % over the poles and -60 to +150 % at different heights over the tropics.

Furthermore, these estimates do not take into account the questions of sulfur production for the SRM injection or aeronautical logistics, both of which are substantial. The estimated numbers are certainly based on the ECHAM-HAM calculations including all of the model uncertainties discussed above. We have not considered indirect effects which may occur under high injection conditions from radiation and dynamical changes. Finally, a changing QBO may alter tracer transport, which feeds back into aerosol microphysics and radiative forcing due to the different aerosol distribution (Aquila et al., 2014).

5 Conclusions

We have considered whether or not SO₂ injections into the stratosphere can theoretically counteract future anthropogenic CO₂ forcings as described in the RCP8.5 scenario. We investigated the efficiency of sulfur SRM, the ratio of TOA forcing to injection rate, with increasing SO₂ injections, as well as the influence of the size of the injection area. Our results show that the TOA forcing, resulting from increasing injection rate of up to 100 Tg(S) yr⁻¹, follows an exponential decay. For the chosen experiment design, injection into one grid box at 60 hPa height, the fit to this curve converges to -65 W m⁻² with an estimated uncertainty of ±15 %. This limit is far from currently estimated injection rates.

Overall, changing the injection flux via increasing the injection rate or the size of the injection area changes the efficiency. Increasing the total injected amount, for example from 10 to 50 Tg(S) yr⁻¹, increases the injection flux and the absolute forcing values, but reduces the forcing to injection ratio, thus decreasing the efficiency. Increasing the injection flux per area by injecting into a smaller area, for example into a box instead of along the Equator, or increasing the flux by shortening the injection time, for example, from continuous to pulsed injections, both result in increases to the absolute forcing and also the forcing efficiency. In both cases the nucleated particles are less evenly distributed. The consequences are changes in aerosol microphysical processes caused by the reduced availability of small particles outside of the injection area and period. Consequently, the resulting

particle size is smaller and scattering of SW radiation is more effective.

The increase in efficiency results from an increase in injection height. Comparing this result to previous studies on the efficiency of injection strategies shows very similarly simulated global sulfate burdens, but also reveals some differences. The strength and location of the subtropical transport barrier, as well as poleward transport to high latitudes, influence the simulated meridional aerosol distribution and contribute, therefore, to different model responses.

The limit of SO₂ injections provided here will differ from a possible limit calculated by other models and should, therefore, not be taken as an absolute value. We described briefly the impact of tracer transport, aerosol microphysical schemes and stratospheric dynamics. A clear answer may be gained by a coordinated comparison of results on the microphysical evolution and the transport of a volcanic cloud obtained from the different models. In turn these results can be compared directly to empirical data. Such an approach is planned within the SPARC initiative SSIRC (www.sparc-ssirc.org) and partly within upcoming GeoMIP studies.

The decreasing efficiency rate of sulfate SRM for higher sulfur emission has already fostered the discussion of alternative approaches. Similar to the injection of SO₂, aerosol injections could also be considered. Ferraro and Charlton-Oerez (2011) studied the impact of limestone, titania (TiO₂) and soot. Soot has a large greenhouse effect, which reduces its efficiency and the simulated forcing of titania showed strong dependencies on the particle size with even positive forcing. Following Weisenstein and Keith (2015) any solid aerosol introduced into the stratosphere would grow via coagulation and accumulation with the consequence of large uncertainties on simulated results. Alternative SRM designs like regional implementation (e.g., Haywood et al., 2013) or reducing only the rate of temperature increase (e.g., MacMartin et al., 2015) would require different amounts of SO₂ injection in a RCP8.5 scenario. In addition to the above-described technical limitations, the negative side effects of sulfur SRM on society and the environment might also set a necessary limit, e.g., to limit the impact on ozone levels, sky brightness and changes in precipitation.

Acknowledgements. We thank Peter Irvine, Sebastian Rast, Alan Robock and Kai Zhang for inspiring discussions, Stefan Kinne and Ian Bytheway for valuable comments at different stages of the paper, three anonymous reviewers for their helpful suggestions and Rene Hommel, Jan Harri Kokkola and Hanna Vehkamäki for their earlier help to modify HAM. This work is a contribution to the German DFG-funded Priority Program Climate Engineering: Risks, Challenges, Opportunities? (SPP 1689). U. Niemeier is supported by the SPP 1689 within the project CEIBRAL. C. Timmreck acknowledges funding from the BMBF project MIKLIP (FKZ:01LP1130A). The simulations were performed at the Deutsches Klima Rechenzentrum (DKRZ) computing facilities.

Further information about the data is available at: <http://www.mpimet.mpg.de/en/staff/ulrike-niemeier/geoengineering/data.html>.

The article processing charges for this open-access publication were covered by the Max Planck Society.

Edited by: B. Kravitz

References

- Aquila, V., Garfinkel, C. I., Newman, P., Oman, L. D., and Waugh, D. W.: Modifications of the quasi-biennial oscillation by a geoengineering perturbation of the stratospheric aerosol layer, *Geophys. Res. Lett.*, 41, 1738–1744, doi:10.1002/2013GL058818, 2014.
- Bekki, S., Pyle, J. A., Zhong, W., Haigh, R. T. J. D., and Pyle, D. M.: The role of microphysical and chemical processes in prolonging the climate forcing of the Toba eruption, *Geophys. Res. Lett.*, 23, 2669–2672, 1996.
- Brasseur, G. and Solomon, S.: *Aeronomy of the Middle Atmosphere*, Springer, 3300 AA Dordrecht, the Netherlands, 2005.
- Budyko, M. I.: *Climatic changes*, American Geophysical Society, Washington, D.C., doi:10.1029/SP010, 1977.
- Cirisan, A., Spichtinger, P., Luo, B. P., Weisenstein, D. K., Wernli, H., Lohmann, U., and Peter, T.: Microphysical and radiative changes in cirrus clouds by geoengineering the stratosphere, *J. Geophys. Res.-Atmos.*, 118, 4533–4548, doi:10.1002/jgrd.50388, 2013.
- Crutzen, P. J.: Albedo enhancement by stratospheric sulfur injections: A contribution to resolve a policy dilemma?, *Climatic Change*, 77, 211–219, 2006.
- English, J. M., Toon, O. B., and Mills, M. J.: Microphysical simulations of sulfur burdens from stratospheric sulfur geoengineering, *Atmos. Chem. Phys.*, 12, 4775–4793, doi:10.5194/acp-12-4775-2012, 2012.
- English, J. M., Toon, O. B., and Mills, M. J.: Microphysical simulations of large volcanic eruptions: Pinatubo and Toba, *J. Geophys. Res.-Atmos.*, 118, 1880–1895, doi:10.1002/jgrd.50196, 2013.
- Ferraro, A. J. a. E. H. and Charlton-Oerez, A.: Stratospheric heating by potential geoengineering aerosols, *Geophys. Res. Lett.*, 38, L24706, doi:10.1029/2011GL049761, 2011.
- Giorgetta, M. A., Manzini, E., Roeckner, E., Esch, M., and Bengtsson, L.: Climatology and forcing of the quasi-biennial oscillation in the MAECHAM5 model, *J. Climate*, 19, 3882–3901, 2006.
- Haywood, J., Jones, A., Bellouin, N., and Stephenson, D.: Asymmetric forcing from stratospheric aerosols impacts Sahelian rainfall, *Nature Climate Change*, 3, 660–665, doi:10.1038/nclimate1857, 2013.
- Heckendorn, P., Weisenstein, D., Fueglistaler, S., Luo, B. P., Rozanov, E., Schraner, M., Thomason, L. W., and Peter, T.: The impact of geoengineering aerosols on stratospheric temperature and ozone, *Environ. Res. Lett.*, 4, 045108, doi:10.1088/1748-9326/4/4/045108, 2009.
- Hommel, R. and Graf, H.: Modelling the size distribution of geoengineered stratospheric aerosols, *Atmos. Sci. Lett.*, 12, 168–175, doi:10.1002/asl.285, 2011.
- Hommel, R., Timmreck, C., and Graf, H. F.: The global middle-atmosphere aerosol model MAECHAM5-SAM2: comparison

- with satellite and in-situ observations, *Geosci. Model Dev.*, 4, 809–834, doi:10.5194/gmd-4-809-2011, 2011.
- Hommel, R., Timmreck, C., Giorgetta, M., and Graf, H.: Quasi-biennial oscillation of the tropical stratospheric aerosol layer, *Atmos. Chem. Phys.*, 15, 5557–5584, doi:10.5194/acp-15-5557-2015, 2015.
- Klimont, Z., Smith, S., and Cofala, J.: The last decade of global anthropogenic sulfur dioxide: 2000–2011 emissions, *Environ. Res. Lett.*, 8, 014003, doi:10.1088/1748-9326/8/1/014003, 2013.
- Kokkola, H., Hommel, R., Kazil, J., Niemeier, U., Partanen, A.-I., Feichter, J., and Timmreck, C.: Aerosol microphysics modules in the framework of the ECHAM5 climate model – intercomparison under stratospheric conditions, *Geosci. Model Dev.*, 2, 97–112, doi:10.5194/gmd-2-97-2009, 2009.
- Kravitz, B., Robock, A., Boucher, O., Schmidt, H., Taylor, K. E., Stenchikov, G., and Schulz, M.: The Geoengineering Model Intercomparison Project (GeoMIP), *Atmos. Sci. Lett.*, 12, 162–167, doi:10.1002/asl.316, 2011.
- Kuebbeler, M., Lohmann, U., and Feichter, J.: Effects of stratospheric sulfate aerosol geo-engineering on cirrus clouds, *Geophys. Res. Lett.*, 39, L23803, doi:10.1029/2012GL053797, 2012.
- Liepert, B. G.: Observed reductions of surface solar radiation at sites in the United States and worldwide from 1961 to 1990, *Geophys. Res. Lett.*, 29, 61.1–61.4, doi:10.1029/2002GL014910, 2002.
- MacMartin, D., Caldeira, K., and Keith, D.: Solar geoengineering to limit the rate of temperature change, *Philos. T. Roy. Soc. A*, 372, 20140 134, doi:10.1098/rsta.2014.0134, 2015.
- McClellan, J., Keith, D. W., and Apt, J.: Cost analysis of stratospheric albedo modification delivery systems, *Environ. Res. Lett.*, 7, 034019, doi:10.1088/1748-9326/7/3/034019, 2012.
- Niemeier, U., Timmreck, C., Graf, H.-F., Kinne, S., Rast, S., and Self, S.: Initial fate of fine ash and sulfur from large volcanic eruptions, *Atmos. Chem. Phys.*, 9, 9043–9057, doi:10.5194/acp-9-9043-2009, 2009.
- Niemeier, U., Schmidt, H., and Timmreck, C.: The dependency of geoengineered sulfate aerosol on the emission strategy, *Atmos. Sci. Lett.*, 12, 189–194, doi:10.1002/asl.304, 2011.
- Niemeier, U., Schmidt, H., Alterskjær, K., and Kristjánsson, J. E.: Solar irradiance reduction via climate engineering – Impact of different techniques on the energy balance and the hydrological cycle, *J. Geophys. Res.*, 118, 11905–11917, doi:10.1002/2013JD020445, 2013.
- Pierce, J. R., Weisenstein, D. K., Heckendorn, P., Peter, T., and Keith, D. W.: Efficient formation of stratospheric aerosol for climate engineering by emission of condensable vapor from aircraft, *Geophys. Res. Lett.*, 37, L18805, doi:10.1029/2010GL043975, 2010.
- Pitari, G., Aquila, V., Kravitz, B., Robock, A., Watanabe, S., Luca, N. D., Genova, G. D., Mancini, E., Tilmes, S., and Cionni, I.: Stratospheric ozone response to sulfate geoengineering: Results from the Geoengineering Model Intercomparison Project (GeoMIP), *J. Geophys. Res.*, 119, 2629–2653, doi:10.1002/2013JD020566, 2013.
- Plumb, R. A. and Bell, R. C.: A model of quasibiennial oscillation on an equatorial beta-plane, *Q. J. Roy. Meteorol. Soc.*, 108, 335–352, 1982.
- Punge, H. J., Konopka, P., Giorgetta, M. A., and Müller, R.: Effects of the quasi-biennial oscillation on low-latitude transport in the stratosphere derived from trajectory calculations, *J. Geophys. Res.*, 114, D03102, doi:10.1029/2008JD010518, 2009.
- Randel, W. J., Wu, F., Russel, J. M., Waters, J. W., and Froidevaux, L.: Ozone and temperature changes in the stratosphere following the eruption of Mount Pinatubo, *J. Geophys. Res.*, 100, 16753–16764, doi:10.1029/95JD01001, 1995.
- Rasch, P. J., Crutzen, P. J., and Coleman, D. B.: Exploring the geoengineering of climate using stratospheric sulfate aerosols: The role of particle size, *Geophys. Res. Lett.*, 35, L02809, doi:10.1029/2007GL032179, 2008.
- Robock, A., Oman, L., and Stenchikov, G. L.: Regional climate responses to geoengineering with tropical and Arctic SO₂ injections, *J. Geophys. Res.*, 113, D16101, doi:10.1029/2008JD010, 2008.
- Roeckner, E., Brokopf, R., Esch, M., Giorgetta, M., Hagemann, S., Kornbluh, L., Manzini, E., Schlese, U., and Schulzweida, U.: Sensitivity of simulated climate to horizontal and vertical resolution in the ECHAM5 atmosphere model, *J. Climate*, 19, 3771–3791, 2006.
- Schmidt, H., Alterskjær, K., Bou Karam, D., Boucher, O., Jones, A., Kristjánsson, J. E., Niemeier, U., Schulz, M., Aaheim, A., Benduhn, F., Lawrence, M., and Timmreck, C.: Solar irradiance reduction to counteract radiative forcing from a quadrupling of CO₂: climate responses simulated by four earth system models, *Earth Syst. Dynam.*, 3, 63–78, doi:10.5194/esd-3-63-2012, 2012.
- Seinfeld, J. H. and Pandis, S. N.: *Atmospheric chemistry and physics: From air pollution to climate change*, Wiley–Interscience, New York, 1998.
- Stier, P., Feichter, J., Kinne, S., Kloster, S., Vignati, E., Wilson, J., Ganzeveld, L., Tegen, I., Werner, M., Balkanski, Y., Schulz, M., Boucher, O., Minikin, A., and Petzold, A.: The aerosol-climate model ECHAM5-HAM, *Atmos. Chem. Phys.*, 5, 1125–1156, doi:10.5194/acp-5-1125-2005, 2005.
- Taylor, K. E., Stouffer, R. J., and Meehl, G. A.: An Overview of CMIP5 and the experiment design, *B. Am. Meteorol. Soc.*, 93, 485–498, doi:10.1175/BAMS-D-11-00094.1, 2012.
- Thomason, L. W., Poole, L. R., and Deshler, T.: A global climatology of stratospheric aerosol surface area density deduced from Stratospheric Aerosol and Gas Experiments II measurements: 1984–1994, *J. Geophys. Res.*, 102, 8967–8976, 1997.
- Tilmes, S., Müller, R., and Salawitch, R.: The sensitivity of polar ozone depletion to proposed geoengineering schemes, *Science*, 320, 1201–1204, doi:10.1126/science.1153966, 2008.
- Tilmes, S., Garcia, R. R., Kinnison, D. E., Gettelman, A., and Rasch, P. J.: Impact of geoengineered aerosols on the troposphere and stratosphere, *J. Geophys. Res.*, 114, D12305, doi:10.1029/2008JD011420, 2009.
- Tilmes, S., Mills, M. J., Niemeier, U., Schmidt, H., Robock, A., Kravitz, B., Lamarque, J.-F., Pitari, G., and English, J. M.: A new Geoengineering Model Intercomparison Project (GeoMIP) experiment designed for climate and chemistry models, *Geosci. Model Dev.*, 8, 43–49, doi:10.5194/gmd-8-43-2015, 2015.
- Timmreck, C.: Three-dimensional simulation of stratospheric background aerosol: First results of a multiannual general circulation model simulation, *J. Geophys. Res.*, 106, 28313–28332, 2001.
- Timmreck, C. and Graf, H.-F.: The initial dispersal and radiative forcing of a Northern Hemisphere mid-latitude super volcano: a model study, *Atmos. Chem. Phys.*, 6, 35–49, doi:10.5194/acp-6-35-2006, 2006.

- Toohey, M., Krüger, K., Niemeier, U., and Timmreck, C.: The influence of eruption season on the global aerosol evolution and radiative impact of tropical volcanic eruptions, *Atmos. Chem. Phys.*, 11, 12351–12367, doi:10.5194/acp-11-12351-2011, 2011.
- Vehkamäki, H., Kulmala, M., Napari, I., Lehtinen, K. E. J., Timmreck, C., Noppel, M., and Laaksonen, A.: An improved parameterization for sulfuric acid water nucleation rates for tropospheric and stratospheric conditions, *J. Geophys. Res.*, 107, 4622–4632, 2002.
- Vignati, E., Wilson, J., and Stier, P.: M7: An efficient size resolved aerosol microphysics module for large-scale aerosol transport models, *J. Geophys. Res.*, 109, D22202, doi:10.1029/2003JD004485, 2004.
- Wan, H., Rasch, P. J., Zhang, K., Kazil, J., and Leung, L. R.: Numerical issues associated with compensating and competing processes in climate models: an example from ECHAM-HAM, *Geosci. Model Dev.*, 6, 861–874, doi:10.5194/gmd-6-861-2013, 2013.
- Weisenstein, D. K. and Keith, D. W.: Solar geoengineering using solid aerosol in the stratosphere, *Atmos. Chem. Phys. Discuss.*, 15, 11799–11851, doi:10.5194/acpd-15-11799-2015, 2015.
- Weisenstein, D. K., Penner, J. E., Herzog, M., and Liu, X.: Global 2-D intercomparison of sectional and modal aerosol modules, *Atmos. Chem. Phys.*, 7, 2339–2355, doi:10.5194/acp-7-2339-2007, 2007.